Terbium Doped Heterometallic Metal-organic Compound with Carboxylate and Imidazole Containing Ligands for Naked-eye Detection of Nitro Containing Antibiotics

Prakash Majee,[a] Arpita Bid,[b,c] Debal Kanti Singha,[d] Chhatan Das,[e] Partha Mahata,[e*] Sujit Sankar Panja,[c*] and Sudip Kumar Mondal,[b*]

[a]Department of Chemistry, UPL University of Sustainable Technology, Vataria-393135, Gujarat, India.

[b]Department of Chemistry, Siksha-Bhavana, Visva-Bharati University, Santiniketan-731235, West Bengal, India. Email: sudip.mondal@visva-bharati.ac.in

[c]Department of Chemistry, National Institute of Technology, Durgapur-713209, West Bengal, India.

Email: sujit.panja@gmail.com

[d]Department of Chemistry, C. V. Raman Global University, Bhubaneswar-752054, Odisha, India.

[e]Department of Chemistry, Jadavpur University, Jadavpur, Kolkata-700 032, West Bengal, India.

Email: parthachem@gmail.com

ELECTRONIC SUPPLEMENTARY INFORMATION

*Corresponding Authors, E-mail: sudip.mondal@visva-bharati.ac.in, sujit.panja@gmail.com, parthachem@gmail.com

Single crystal X-ray diffraction. Suitable single crystals of **1** were carefully selected under an optical microscope and mounted on thin glass fiber carefully. The single crystal data of both the compounds were collected using Bruker D8-Quest diffractometer. The instrument was equipped with Mo Kα (λ=0.71073Å) radiation source and operating voltage of X-ray generator was 50 kV and 1 mA. Diffraction data were collected with ω scan width of 0.5°. Three different setting of φ (0, 90, 180°) were used to collect the total 408 frames, keeping a fixed distance of sample-to-detector at 6.03 cm and the detector position (2θ) was fixed at -25°. The initial indexing, final data sets, and cell refinements were handled by an APEX3 program, while a SAINTPLUS[1] program was utilized for the frame integration and final cell parameter calculation. The multi-scan absorption data was corrected by a SADABS program.[2] We initially solved the structure by SIR 92,[3] and the full matrix least-square method (SHELXL-2016[4]) was used further, which is present in the WinGx suite of programs (Version 1.63.04a).[5, 6] With the help of Fourier maps, we successfully located all the non-hydrogen atoms and refined them anisotropically. Finally, all the hydrogen atoms were fixed at calculated positions and included them in the refinement process using riding model associated with isotropic thermal parameters. The details of the crystal and final refinements are given in the Table S1. CCDC: 2421989 is the crystallographic data for this paper. These data can be obtained free of charge from The Cambridge Crystallographic Data Center (CCDC) via www.ccdc.cam.ac.uk/data_request/cif.

Powder X-ray diffraction. The finely ground samples were used for the powder X-ray diffraction (PXRD) experiments on a Bruker D8 Discover instrument using Cu Kα radiation within the 2θ range of 5-50º (see supporting information, Figure S1). The PXRD patterns of compound **1** are in good agreement with the simulated PXRD pattern generated based on the structure determined using the single-crystal XRD data of compound **1** which indicates the compound's phase purity.

Thermal Stability. Thermogravimetric analysis was performed using a TA Discovery SDT 650 DSC/TGA instrument under a nitrogen atmosphere condition (flow rate = 20 mL min^{-1}) between 25 ºC and 900 ºC with a heating rate = 20ºC min^{-1}. TGA curves revealed that a constant weight loss of 14.40% occurred in the temperature range of 25-254 °C, corresponding to the loss of lattice H_2O molecules in the channel and coordinated H_2O molecules (calculated 14.77%). After that weight loss is due to the decomposition of the framework (see supporting information, Figure S2).

FTIR measurements. FTIR measurements were performed between 400 cm^{-1} and 4000 cm^{-1} using a Bruker ALPHA II spectrometer in attenuated total reflectance (ATR) mode. IR spectra of compound **1** and compound **1:Tb** (see supporting information, Figure S3 and S4) support the crystal structure.

Table S1: Crystal data and structure refinement parameters for compound $[YSr(pda)_3(H_2O)_4]\cdot Him\cdot 3H_2O$, **1**.

Empirical formula	$C_{24}H_{14}N_5O_{19}Sr_1Y_1$
Formula weight	852.93
Crystal system	Triclinic
Space group	*P*-1 (No. 2)
a (Å)	10.0461(13)
b (Å)	10.2685(14)
c (Å)	16.065(2)
α (deg)	81.418(4)
β (deg)	72.104(4)
γ (deg)	88.928(5)
Volume ($Å^3$)	1558.7(4)
Z	2
T (K)	273(2)
ρ_{calc} ($g\ cm^{-3}$)	1.817
μ (mm^{-1})	3.657
θ range (deg)	2.131 to 27.158
λ (Mo Kα) (Å)	0.71073
R indices [I>2σ(I)]	$R_1 = 0.0694$, $wR_2 = 0.1774$
R indices [(all data)]	$R_1 = 0.0807$, $wR_2 = 0.1832$

$R_1 = \Sigma\ ||F_0|-|F_c|| / \Sigma\ |F_0|$; $wR_2 = \{\Sigma[w(F_0^2 - F_c^2)^2] / \Sigma[w(F_0^2)^2]\}^{1/2}$. $w = 1/[\sigma^2(F_0)^2 + (aP)^2 + bP]$, $P = [max.(F_0^2,0) + 2(F_c)^2]/3$, where a = 0.0591 and b = 12.9486

Table S2: Selected bond distances (Å) observed in $[YSr(pda)_3(H_2O)_4]\cdot Him\cdot 3H_2O$, **1**.

Bond	Distances, Å	Bond	Distances, Å
Y(1)-O(5)	2.367(5)	Y(1)-N(2)	2.480(5)
Y(1)-O(1)	2.382(5)	Sr(1)-O(12)	2.525(5)
Y(1)-O(11)	2.384(4)	Sr(1)-O(14)	2.545(7)
Y(1)-O(9)	2.405(4)	Sr(1)-O(10)#1	2.549(4)
Y(1)-O(3)	2.410(4)	Sr(1)-O(8)#2	2.570(5)
Y(1)-O(7)	2.419(4)	Sr(1)-O(13)	2.602(8)
Y(1)-N(3)	2.463(5)	Sr(1)-O(15A)/O(15B)	2.769(11)/2.654(11)
Y(1)-N(1)	2.469(5)	Sr(1)-O(16)#2	2.656(7)

Symmetry transformations used to generate equivalent atoms: #1 x-1,y,z #2 -x,-y+1,-z+2

Table S3: Selected bond angles observed in $[YSr(pda)_3(H_2O)_4]\cdot Him\cdot 3H_2O$, **1**.

Angle	Amplitude (º)	Angle	Amplitude (º)
O(5)-Y(1)-O(1)	78.54(18)	O(12)-Sr(1)-O(14)	78.4(2)
O(5)-Y(1)-O(11)	147.38(17)	O(12)-Sr(1)-O(10)#1	74.80(15)
O(1)-Y(1)-O(11)	90.73(18)	O(14)-Sr(1)-O(10)#1	79.19(19)
O(5)-Y(1)-O(9)	79.01(16)	O(12)-Sr(1)-O(8)#2	146.87(17)
O(1)-Y(1)-O(9)	78.67(16)	O(14)-Sr(1)-O(8)#2	89.6(2)
O(11)-Y(1)-O(9)	129.36(15)	O(10)#1-Sr(1)-O(8)#2	72.65(16)
O(5)-Y(1)-O(3)	88.24(18)	O(12)-Sr(1)-O(13)	92.8(2)
O(1)-Y(1)-O(3)	129.89(16)	O(14)-Sr(1)-O(13)	151.2(2)
O(11)-Y(1)-O(3)	75.13(17)	O(10)#1-Sr(1)-O(13)	72.0(2)
O(9)-Y(1)-O(3)	145.82(16)	O(8)#2-Sr(1)-O(13)	83.0(2)
O(5)-Y(1)-O(7)	128.94(17)	O(12)-Sr(1)-O(15B)	132.8(2)
O(1)-Y(1)-O(7)	145.86(18)	O(14)-Sr(1)-O(15B)	90.3(3)
O(11)-Y(1)-O(7)	74.88(17)	O(10)#1-Sr(1)-O(15B)	148.1(2)
O(9)-Y(1)-O(7)	86.80(16)	O(8)#2-Sr(1)-O(15B)	77.3(2)
O(3)-Y(1)-O(7)	76.80(16)	O(13)-Sr(1)-O(15B)	114.8(3)
O(5)-Y(1)-N(3)	137.68(17)	O(12)-Sr(1)-O(16)#2	75.7(2
O(1)-Y(1)-N(3)	73.95(17)	O(14)-Sr(1)-O(16)#2	93.7(3)
O(11)-Y(1)-N(3)	64.86(16)	O(10)#1-Sr(1)-O(16)#2	150.4(2)
O(9)-Y(1)-N(3)	64.61(15)	O(8)#2-Sr(1)-O(16)#2	136.5(2)
O(3)-Y(1)-N(3)	134.06(17)	O(13)-Sr(1)-O(16)#2	110.9(3)
O(7)-Y(1)-N(3)	71.91(17)	O(15B)-Sr(1)-O(16)#2	59.3(3)
O(5)-Y(1)-N(1)	75.68(17)	O(12)-Sr(1)-O(15A)	122.1(3)
O(1)-Y(1)-N(1)	65.37(17)	O(14)-Sr(1)-O(15A)	62.6(4)
O(11)-Y(1)-N(1)	71.86(17)	O(10)#1-Sr(1)-O(15A)	130.5(3)
O(9)-Y(1)-N(1)	139.21(17)	O(8)#2-Sr(1)-O(15A)	76.6(3)
O(3)-Y(1)-N(1)	64.53(17)	O(13)-Sr(1)-O(15A)	140.6(4)
O(7)-Y(1)-N(1)	133.92(17)	O(16)#2-Sr(1)-O(15A)	66.8(3)
N(3)-Y(1)-N(1)	118.82(17)	O(12)-Sr(1)-O(15B)#2	88.8(2)
O(5)-Y(1)-N(2)	64.70(17)	O(14)-Sr(1)-O(15B)#2	144.7(2)
O(1)-Y(1)-N(2)	136.05(18)	O(10)#1-Sr(1)-O(15B)#2	129.1(2)
O(11)-Y(1)-N(2)	133.19(18)	O(8)#2-Sr(1)-O(15B)#2	116.7(2)
O(9)-Y(1)-N(2)	71.65(17)	O(13)-Sr(1)-O(15B)#2	60.9(3)
O(3)-Y(1)-N(2)	74.22(17)	O(15B)-Sr(1)-O(15B)#2	74.5(4)
O(7)-Y(1)-N(2)	64.26(17)	O(16)#2-Sr(1)-O(15B)#2	51.1(3)

N(3)-Y(1)-N(2)	118.39(17)	O(15A)-Sr(1)-O(15B)#2	99.2(4)
N(1)-Y(1)-N(2)	122.69(17)		

Symmetry transformations used to generate equivalent atoms: #1 x-1,y,z #2 -x,-y+1,-z+2

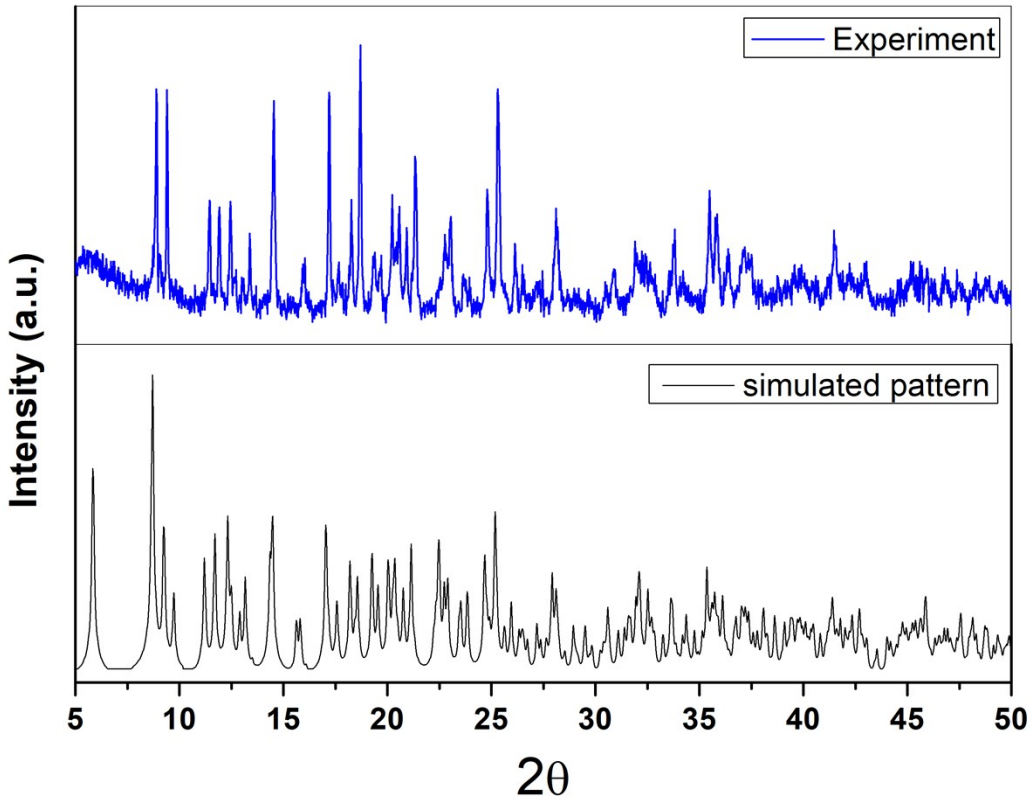

Fig. S1: Powder XRD (CuKα) patterns of $[YSr(PDA)_3(H_2O)_4]\cdot Him\cdot 3H_2O$, **1**: (a) simulated from single crystal X-ray data (b) experimental.

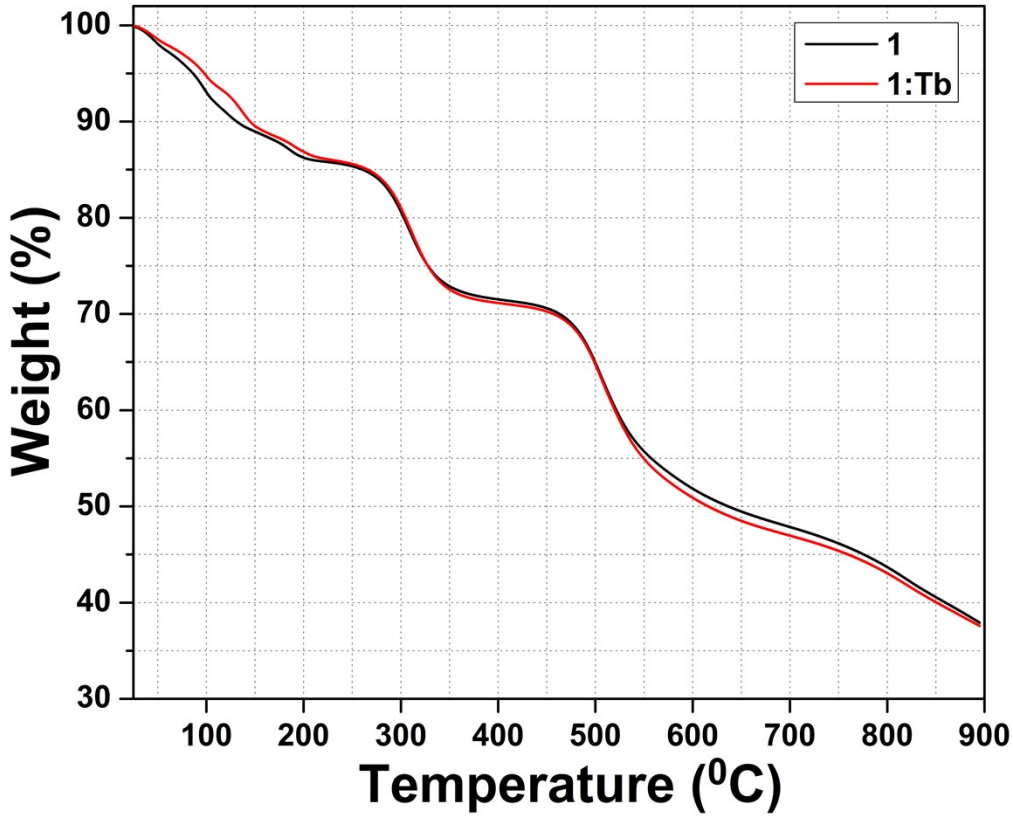

Fig. S2: Thermogravimetric analysis (TGA) of $[YSr(PDA)_3(H_2O)_4]\cdot Him\cdot 3H_2O$, **1**, and $[Y_{0.9}Tb_{0.1}Sr(PDA)_3(H_2O)_4]\cdot Him\cdot 3H_2O$, **1:Tb** in nitrogen atmosphere.

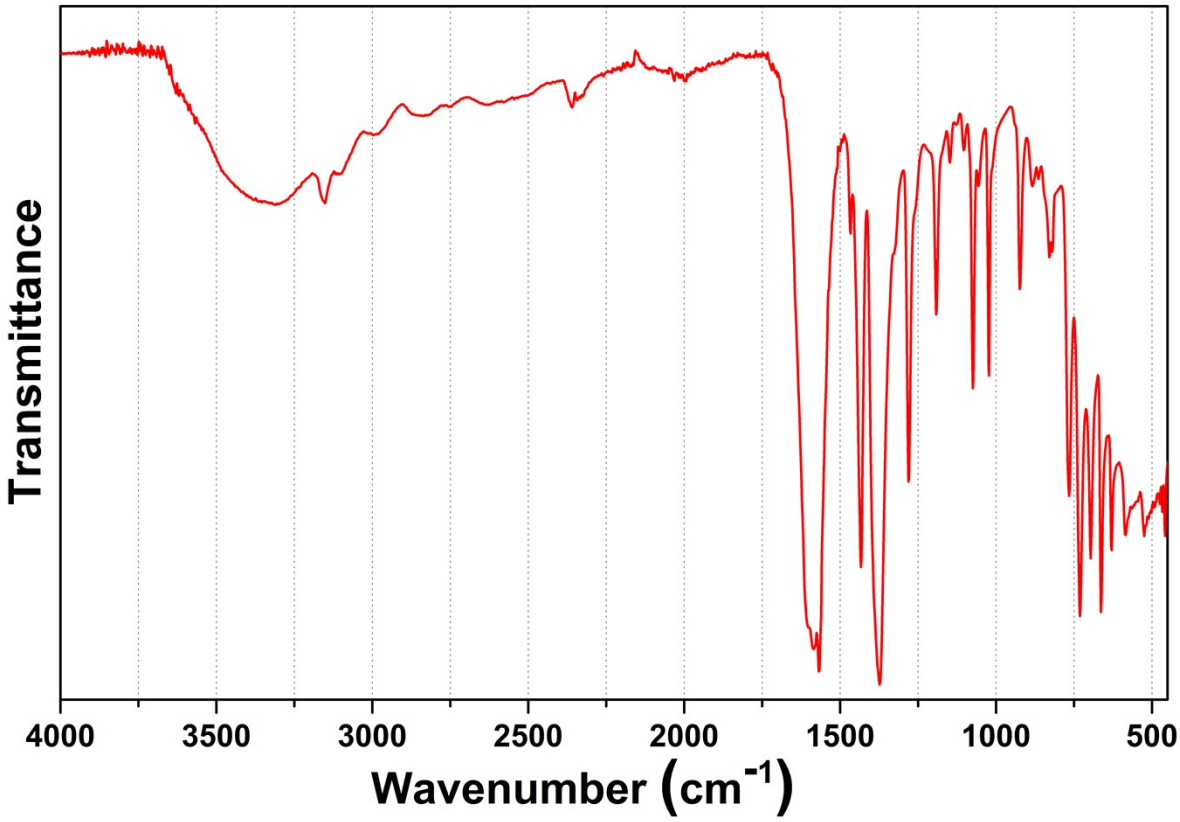

Fig. S3: IR spectrum of $[YSr(PDA)_3(H_2O)_4]\cdot Him\cdot 3H_2O$, **1.**

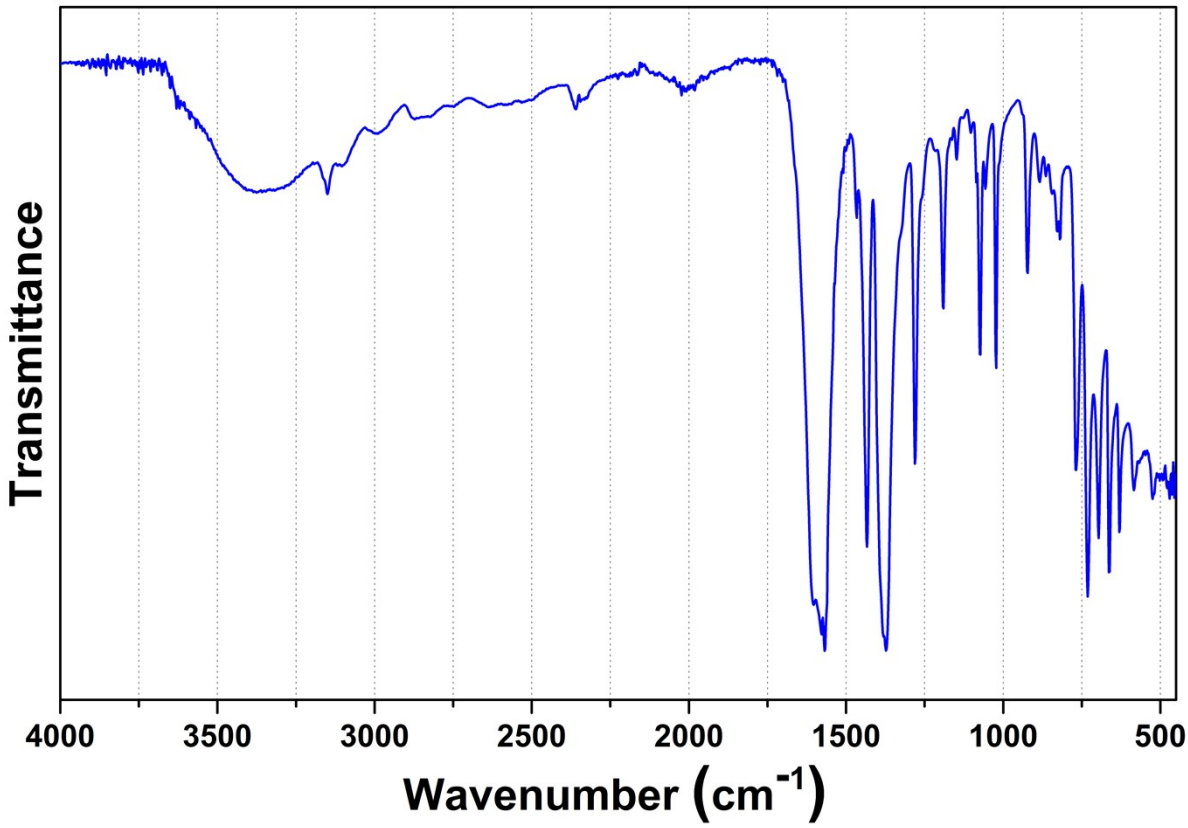

Fig. S4: IR spectrum of $[Y_{0.9}Tb_{0.1}Sr(PDA)_3(H_2O)_4]\cdot Him\cdot 3H_2O$, **1:Tb.**

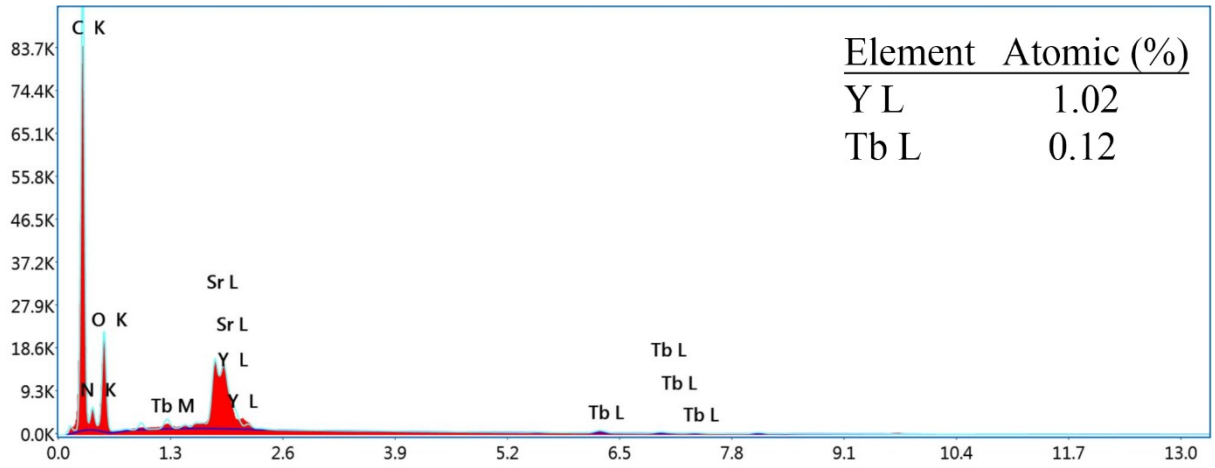

Fig. S5: Representative EDX of compound **1:Tb**. Note the presence of Y and Tb are in molar ratio of ~ 9:1.

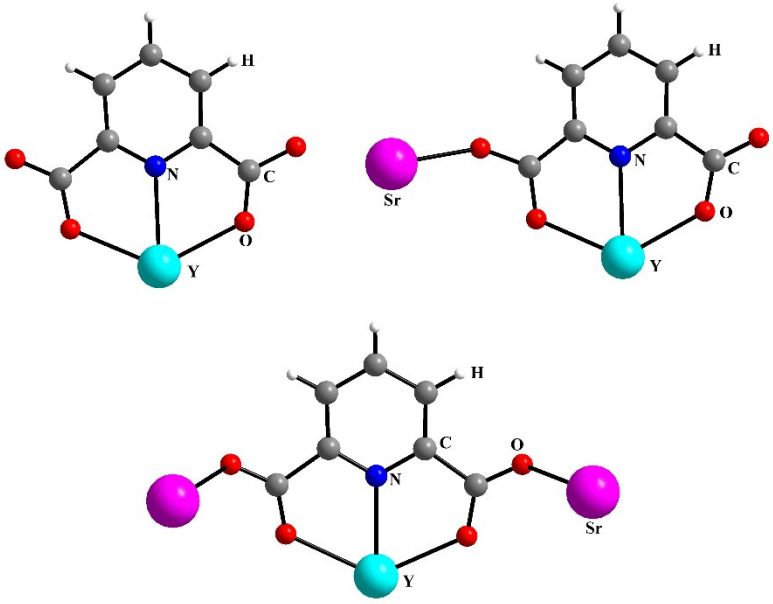

Fig. S6: Three different types of coordination modes of PDA ligands observed in $[YSr(PDA)_3(H_2O)_4]\cdot Him\cdot 3H_2O$, compound **1**.

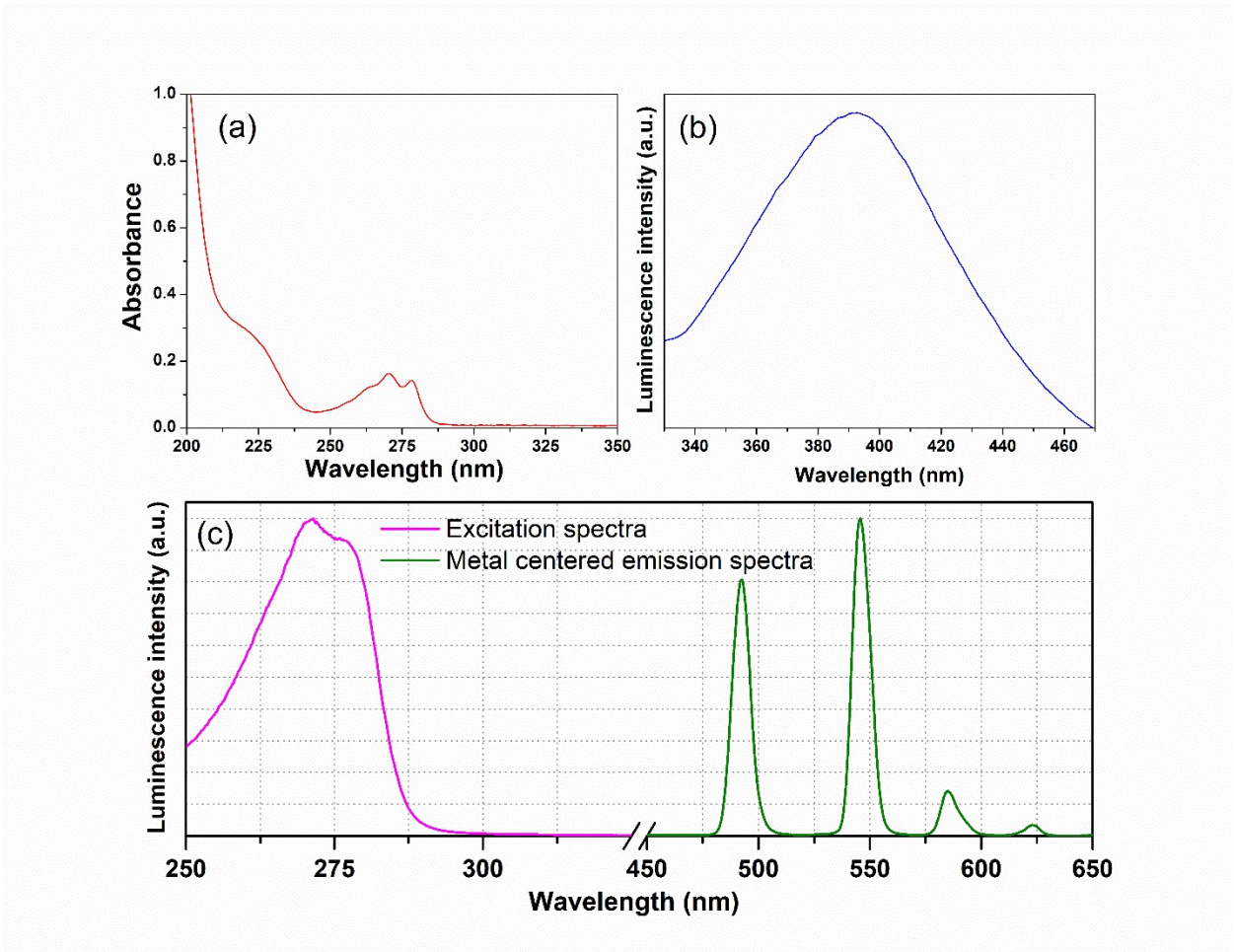

Fig. S7: (a) Absorption, (b) ligand centered emission spectra (c) excitation and metal centered emission spectra of compound **1:Tb**.

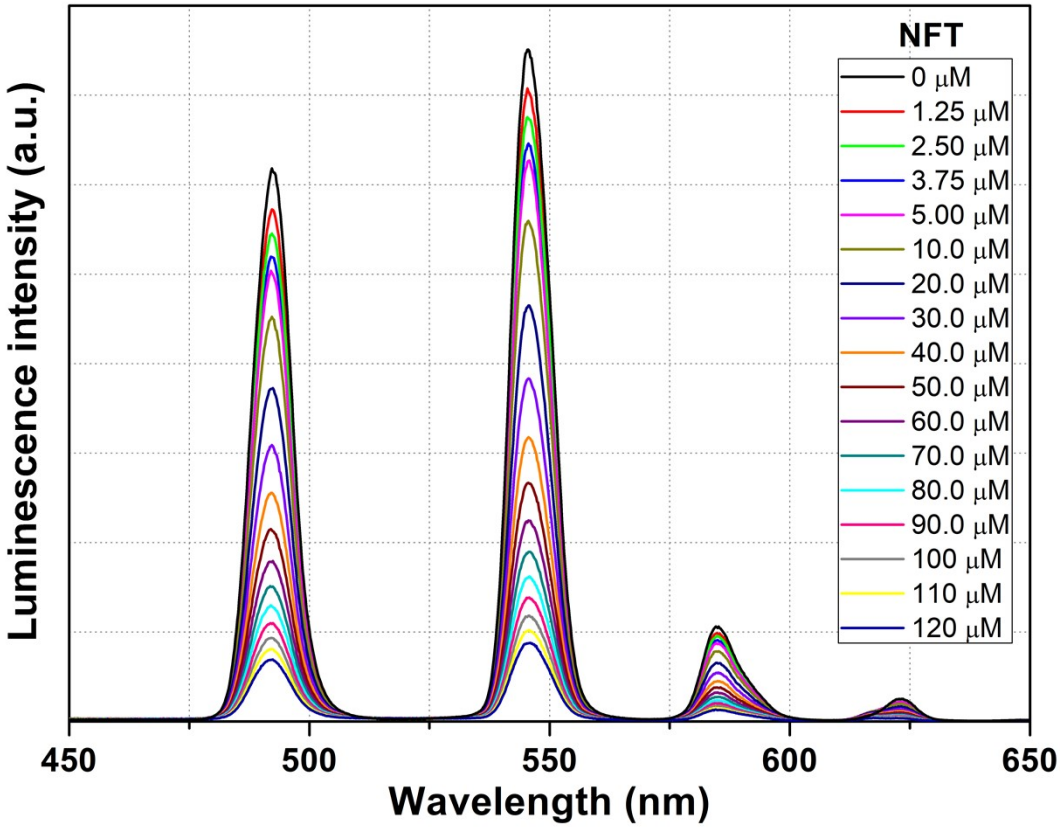

Fig. S8: Emission spectra of compound **1:Tb** solution in water upon incremental addition of acetonitrile solution of nitrofurantoin (NFT) solution (λ_{ex} = 280 nm). Final concentration of NFT in the medium is indicated in the ligand.

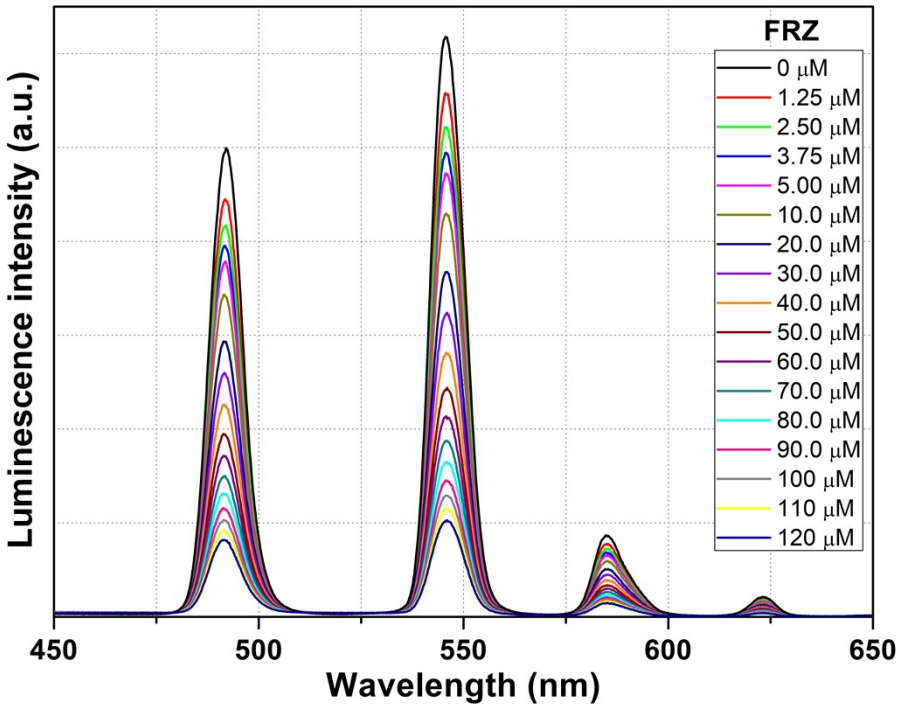

Fig. S9: Emission spectra of compound **1:Tb** solution in water upon incremental addition of acetonitrile solution of furazolidone (FRZ) solution (λ_{ex} = 280 nm). Final concentration of FRZ in the medium is indicated in the ligand.

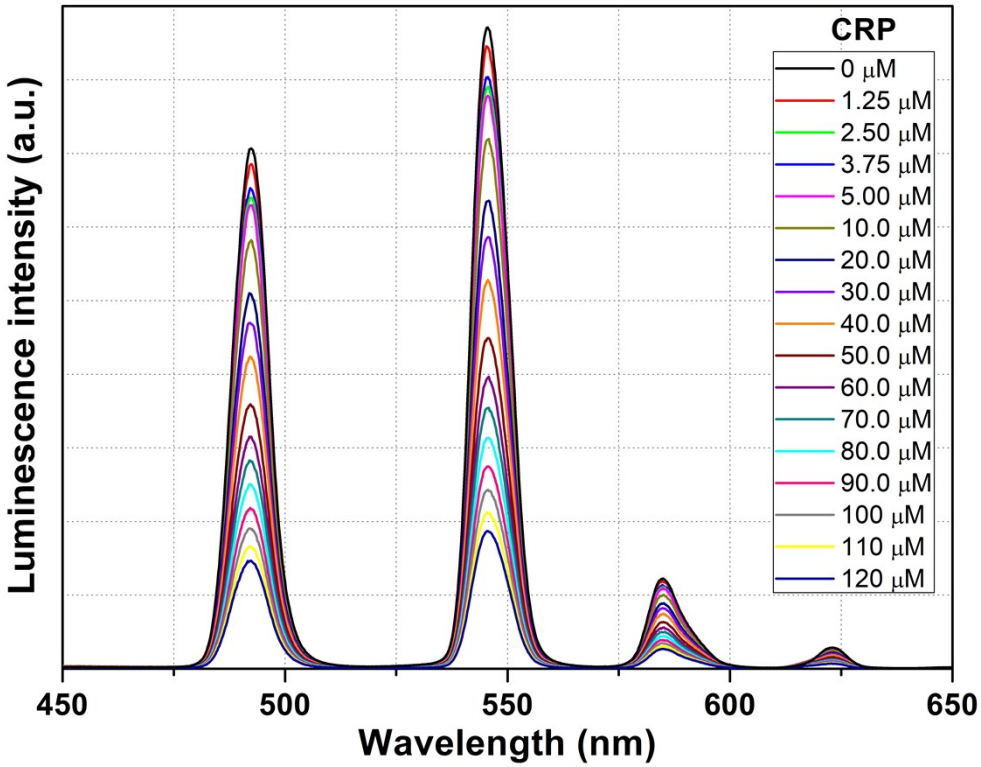

Fig. S10: Emission spectra of compound **1:Tb** solution in water upon incremental addition of acetonitrile solution of chloramphenicol (CRP) solution (λ_{ex} = 280 nm). Final concentration of CRP in the medium is indicated in the ligand.

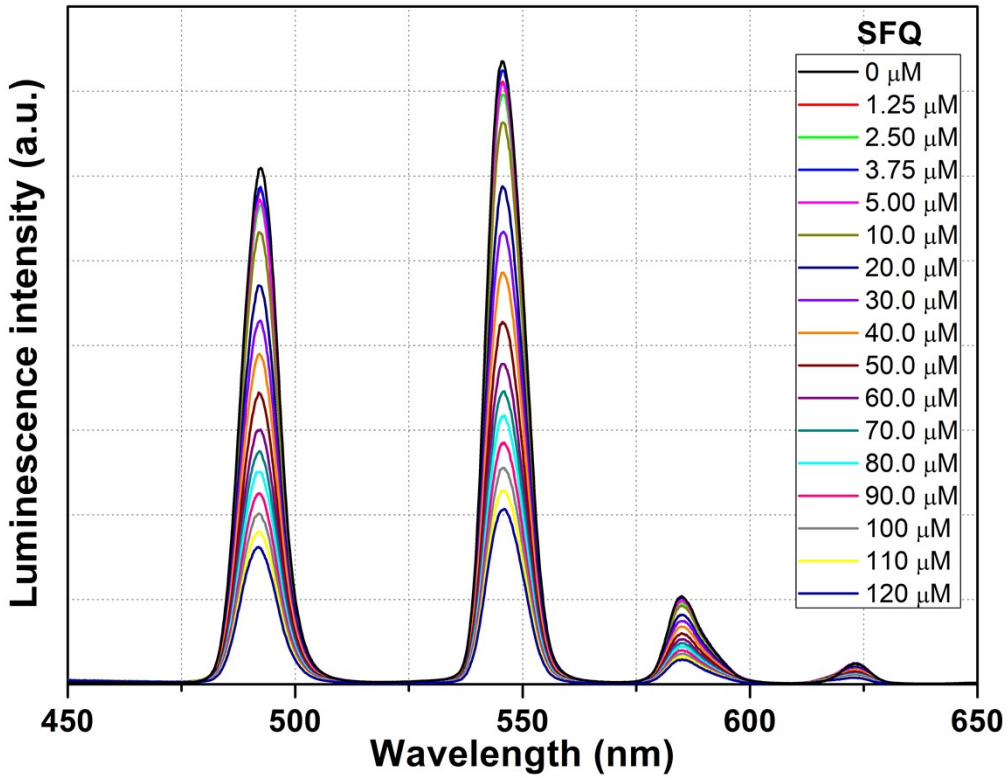

Fig. S11: Emission spectra of compound **1:Tb** solution in water upon incremental addition of acetonitrile solution of sulfaquinoxaline (SFQ) solution (λ_{ex} = 280 nm). Final concentration of SFQ in the medium is indicated in the ligand.

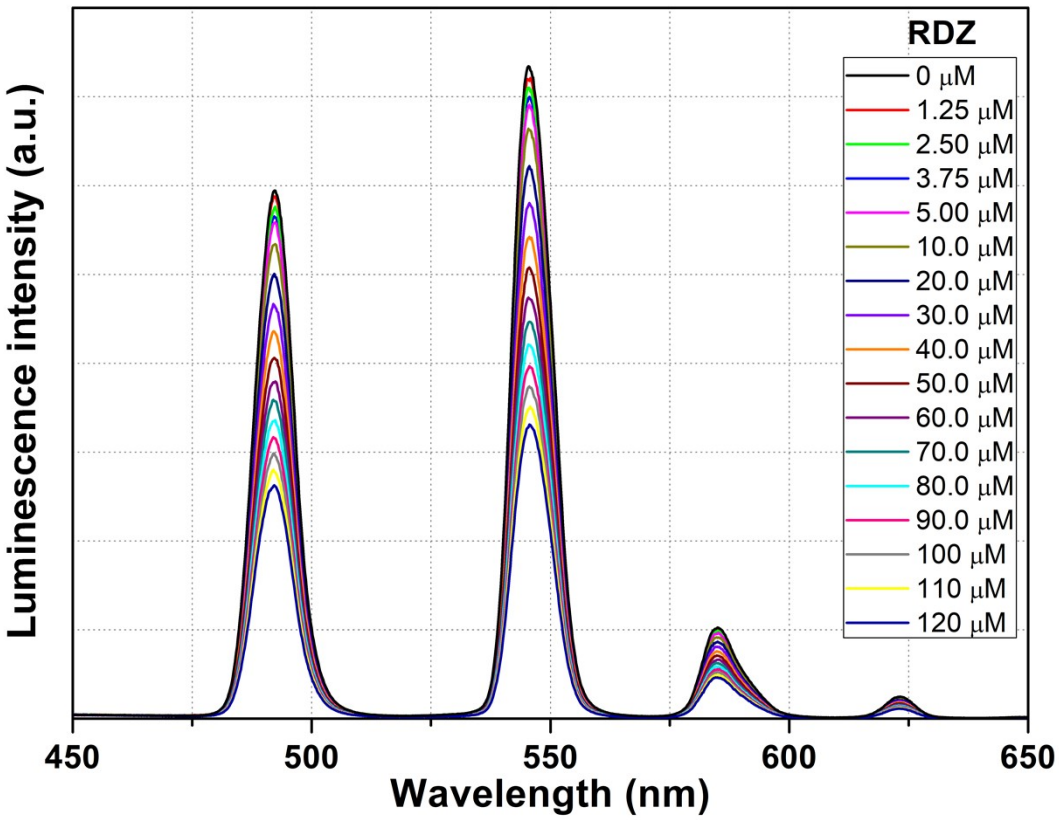

Fig. S12: Emission spectra of compound **1:Tb** solution in water upon incremental addition of acetonitrile solution of ronidazole (RDZ) solution (λ_{ex} = 280 nm). Final concentration of RDZ in the medium is indicated in the ligand.

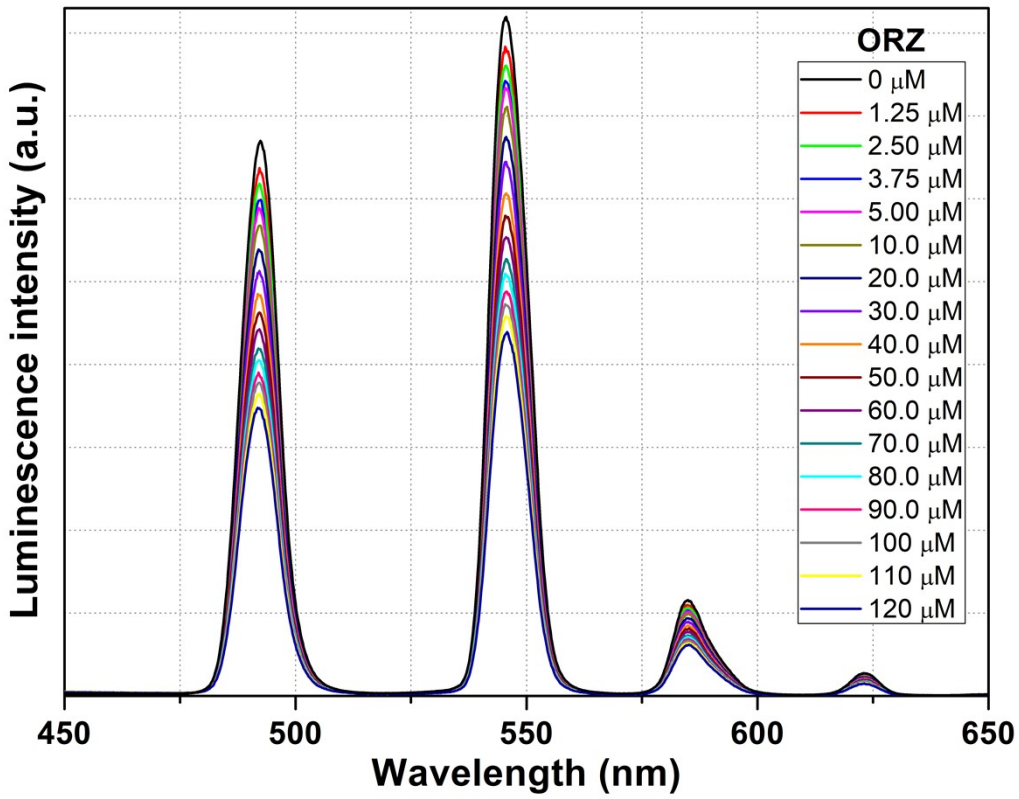

Fig. S13: Emission spectra of compound **1:Tb** solution in water upon incremental addition of acetonitrile solution of ornidazole (ORZ) solution (λ_{ex} = 280 nm). Final concentration of NFZ in the medium is indicated in the ligand.

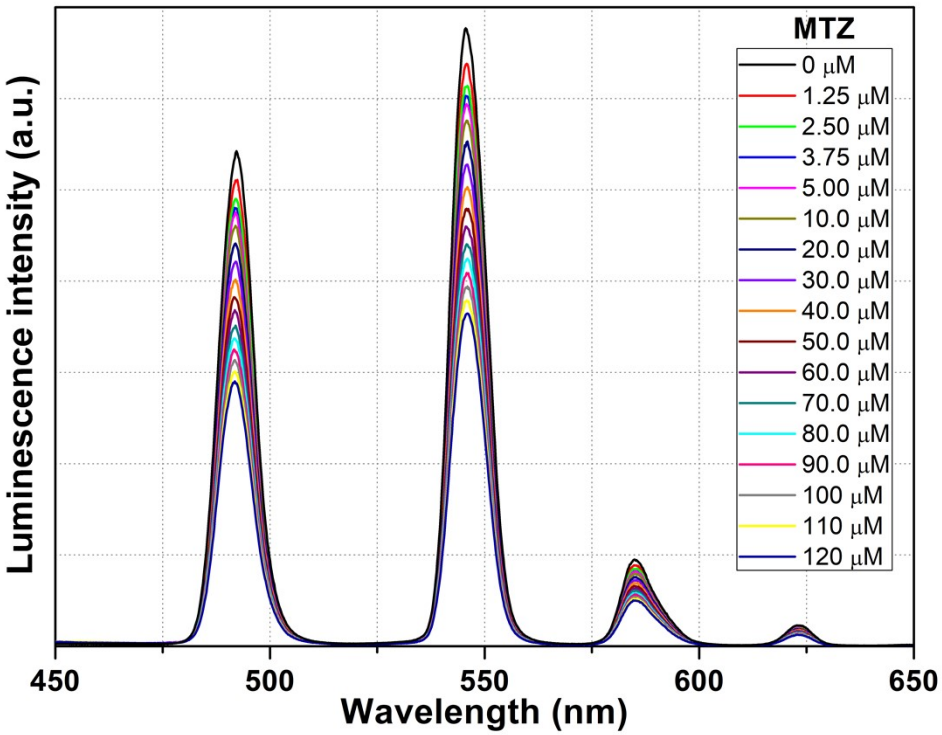

Fig. S14: Emission spectra of compound **1:Tb** solution in water upon incremental addition of acetonitrile solution of metronidazole (MTZ)solution (λ_{ex} = 280 nm). Final concentration of MTZ in the medium is indicated in the ligand.

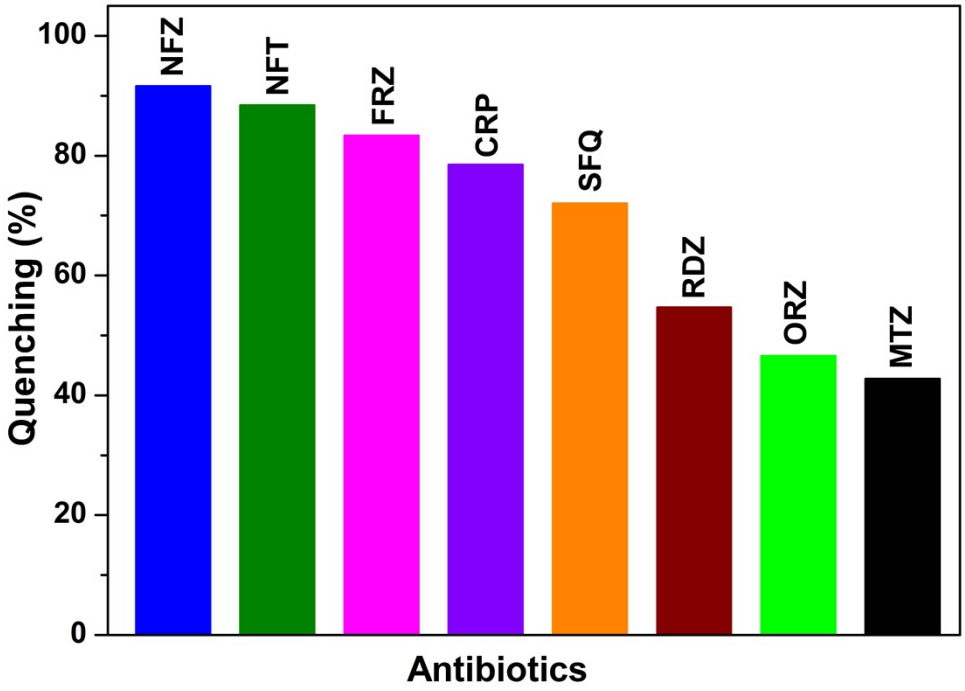

Fig. S15: Quenching percentage of compound **1:Tb** in water after the addition of 120 μM antibiotics solution.

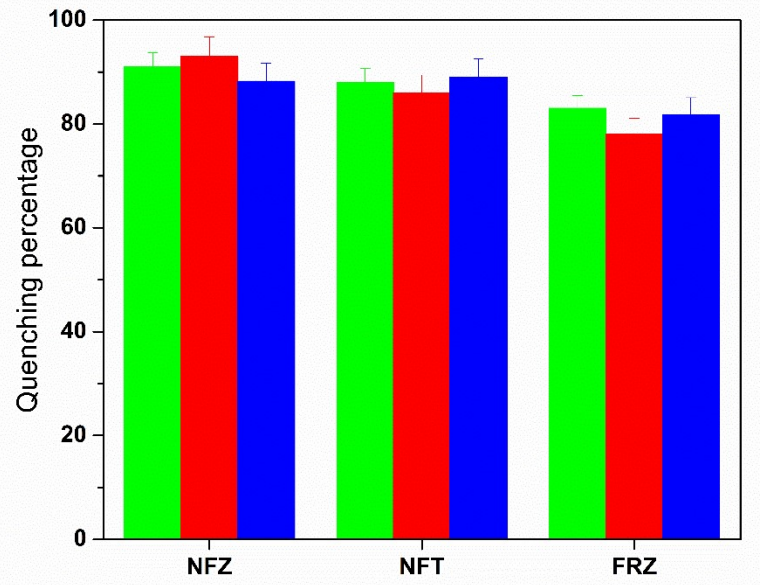

Fig. S16: Quenching percentage of compound **1:Tb** in water after the addition of 120 μM antibiotics solution at 4 h intervals in a day.

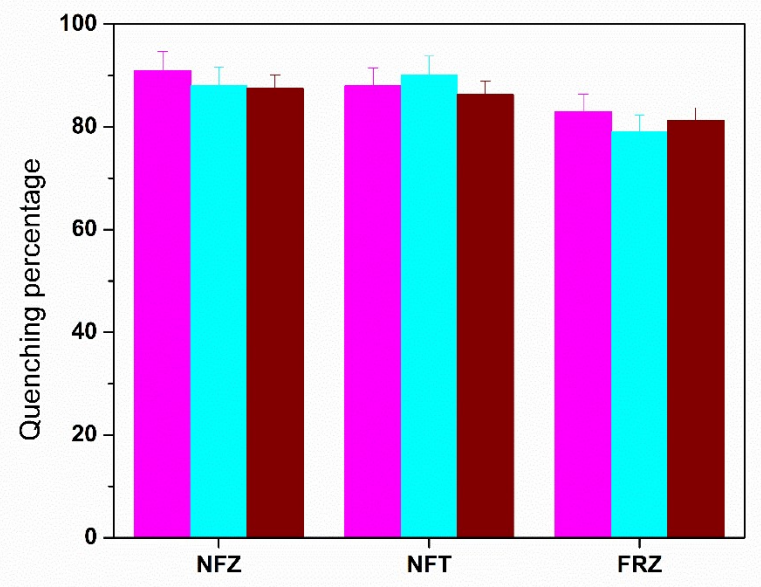

Fig. S17: Quenching percentage of compound **1:Tb** in water after the addition of 120 μM antibiotics solution on three consecutive days.

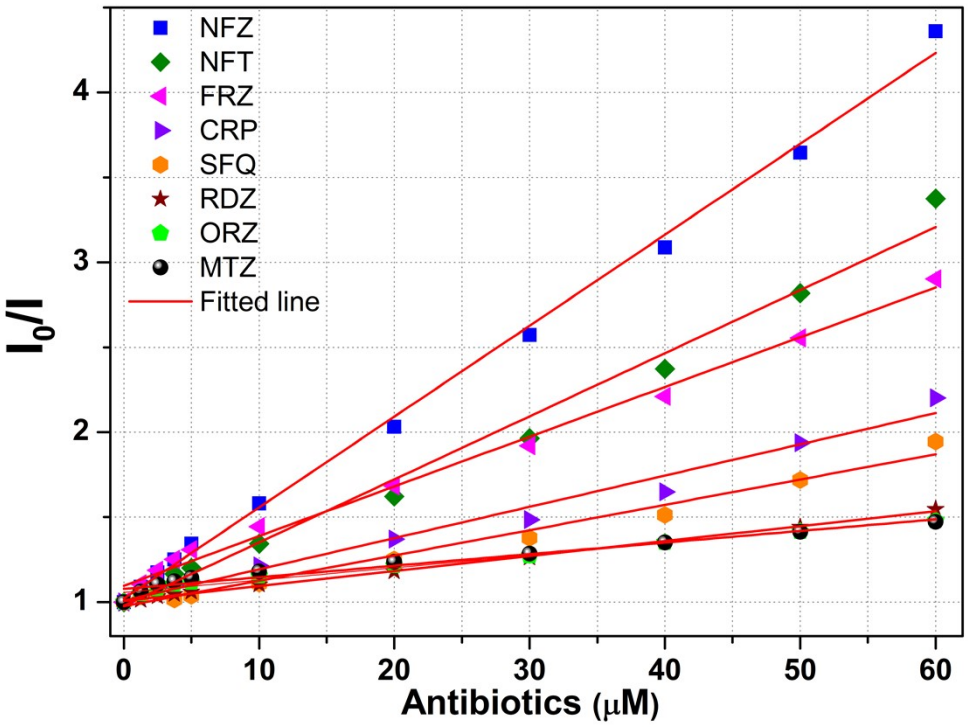

Fig. S18: Plot of I_0/I of compound **1:Tb** (at 545 nm) *vs* concentration of antibiotics [A] in lower concentration range (up to 60 μM).

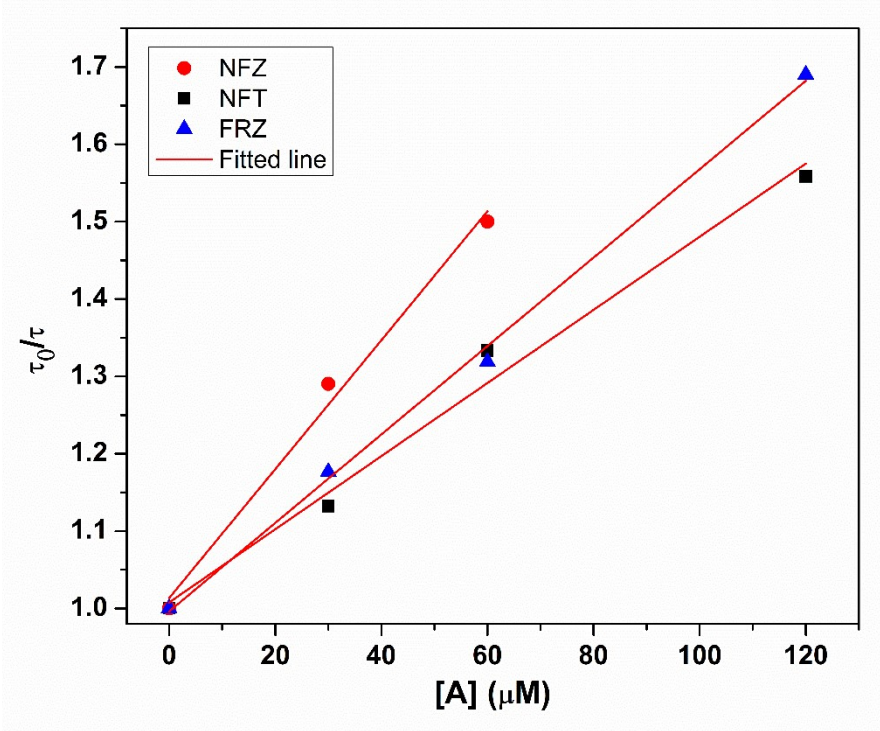

Fig. S19: Plot of τ_0/τ of compound **1:Tb** (at 545 nm) *vs* concentration of antibiotics [A].

Table S4: K_{SV}, K_D, K_S, values of antibiotics.

Antibiotics	$K_{SV}(M^{-1})$	$K_{D(M^{-1})}$	$K_{S(M^{-1})}$
NFZ	5.35×10^4	0.47×10^4	4.88×10^4
NFT	3.71×10^4	0.83×10^4	2.88×10^4
FRZ	2.93×10^4	0.57×10^4	2.36×10^4

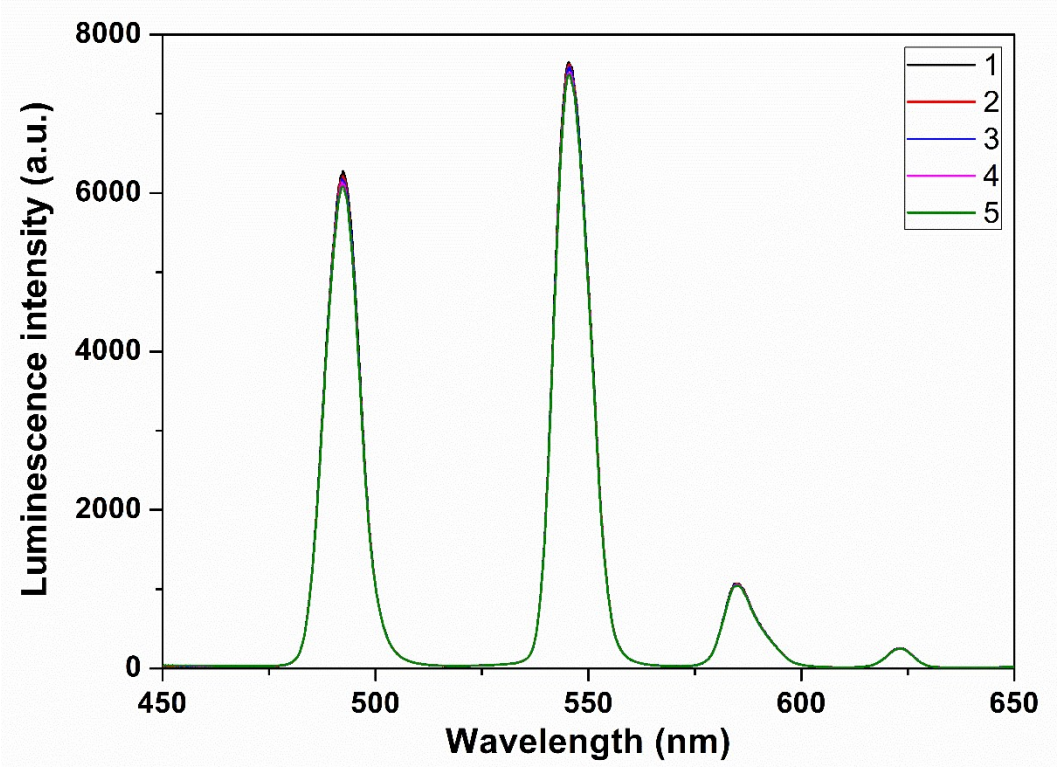

Figure S20: Standard curve of blank readings (5 times) for the determination of LoD.

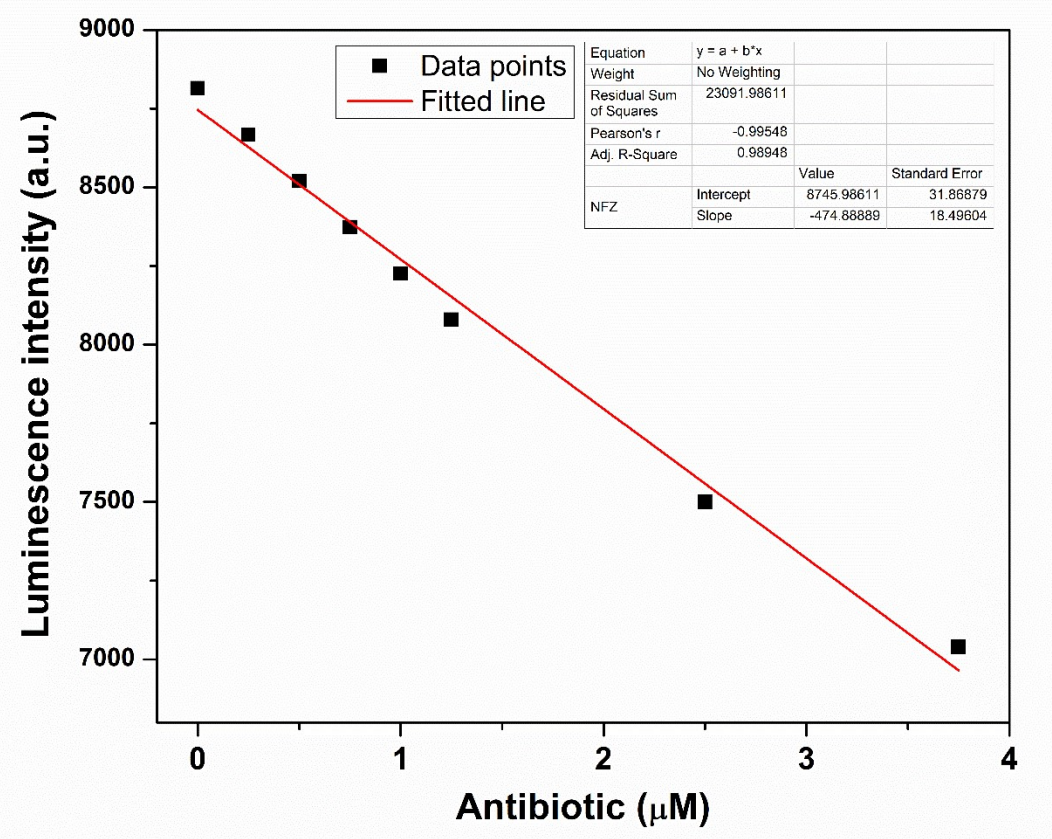

Fig. S21: Linear region of luminescence intensity (at 545 nm) of compound **1:Tb** upon addition of NFZ (R^2 = 0.98948).

Calculation of Detection Limit

Standard Deviation (σ)	78.84
Slope from Graph (m)	475 μM^{-1}

Thus, Limit of Detection (LOD) = $3\sigma/m$ = (3×78.84)/475 =0.49 μM

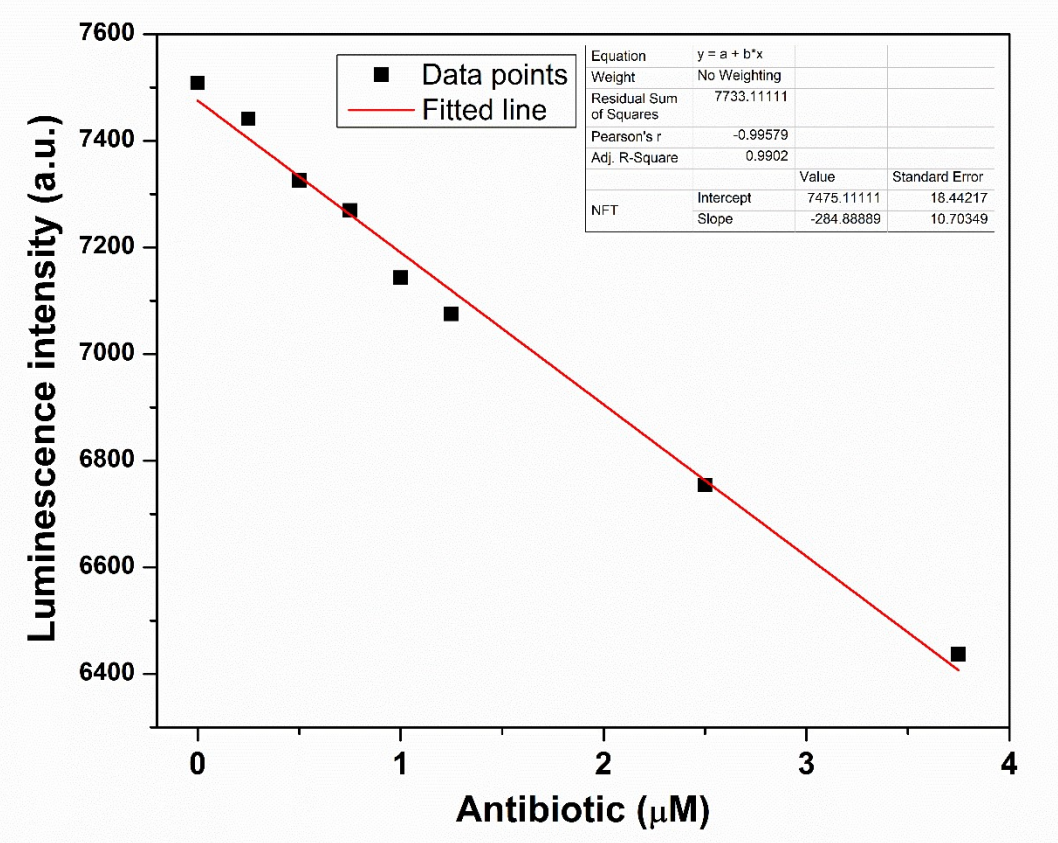

Fig. S22: Linear region of luminescence intensity (at 545 nm) of compound **1:Tb** upon addition of NFT (R^2 = 0.9902).

Calculation of Detection Limit

Standard Deviation (σ)	78.84
Slope from Graph (m)	285 μM^{-1}

Thus, Limit of Detection (LOD) = $3\sigma/m$ = (3×78.84)/285 =0.83 μM

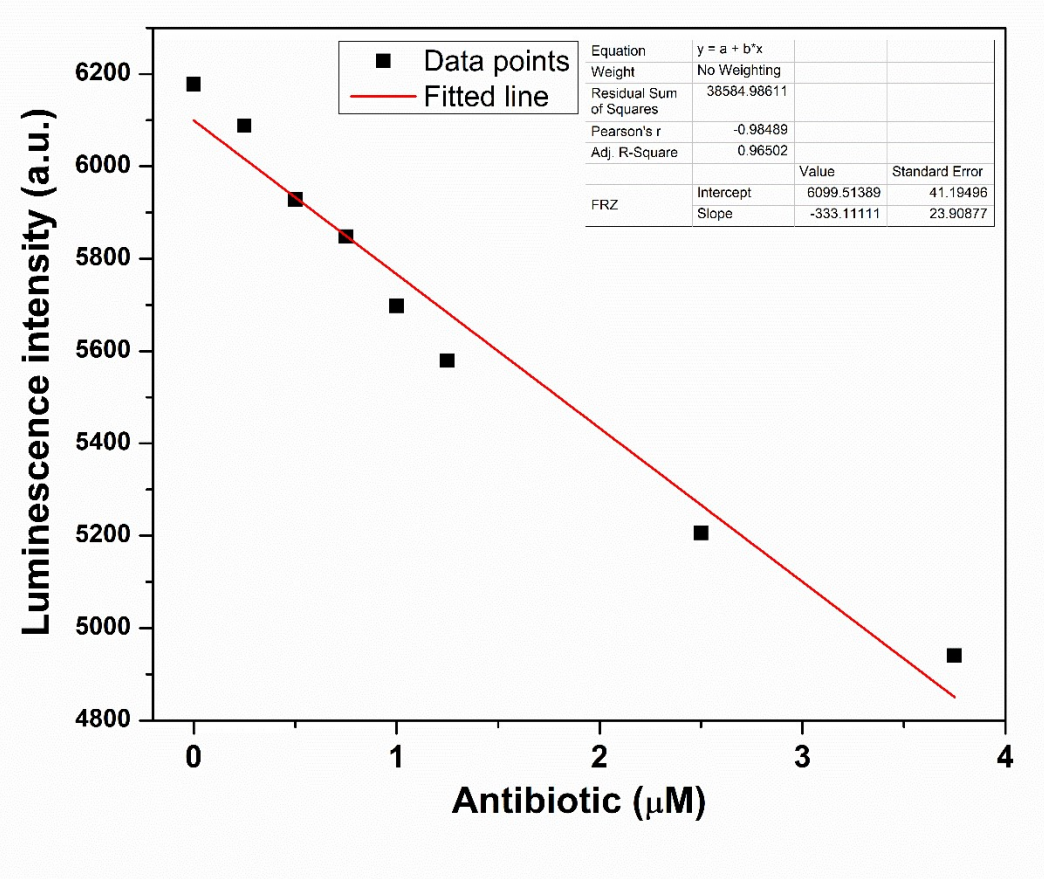

Fig. S23: Linear region of luminescence intensity (at 545 nm) of compound **1:Tb** upon addition of FRZ (R^2 = 0.96502).

Calculation of Detection Limit

Standard Deviation (σ)	78.84
Slope from Graph (m)	333 μM^{-1}

Thus, Limit of Detection (LOD) = $3\sigma/m$ = (3×78.84)/333 =0.71 μM

Table S5: A comparison table of detection limit and K_{SV} value for the nitro-containing antibiotics detection by MOFs

Compounds	Analytes	Limit of detection	Ksv value	Ref
$\{[Tb_2(AIP)_2(H_2O)_{10}]\cdot(AIP)\cdot 4H_2O\}_n$	NFT and NFZ	NFT: 0.30 μM NFZ: 0.35 μM	NFT: 4.0×10^4 M^{-1} NFZ: 2.8×10^4 M^{-1}	[7]
$[Me_2NH_2][Tb_3(dcpcpt)_3(HCOO)]\cdot DMF\cdot 15H_2O$	NFT and NFZ	NA	NFT: 6.69×10^4 M^{-1} NFZ: 5.98×10^4 M^{-1}	[8]
$[Zn_2(TRZ)_2(DBTDC\text{-}O_2)]\cdot DMAc$	NFT and NFZ	NFT: 0.35 μM NFZ: 0.40 μM	NFT: 1.8×10^5 M^{-1} NFZ: 5.2×10^4 M^{-1}	[9]
$\{[Zn_2(Py_2TTz)_2(BDC)_2]\cdot 2(DMF)\cdot 0.5(H_2O)\}_n$	NFZ	0.91 μM	1.7×10^4 M^{-1}	[10]
$\{[Cd_3(TDCPB)\cdot 2DMAc]\cdot DMAc\cdot 4H_2O\}_n$	NFT and NFZ	NA	NFT: 1.05×10^5 M^{-1} NFZ: 7.46×10^4 M^{-1}	[11]
$[Cd(tptc)_{0.5}(o\text{-}bimb)]_n$	NFZ	0.21 μM	4.4×10^4 M^{-1}	[12]
HNU-52	NFT and NFZ	NFT: 0.92 μM NFZ: 0.72 μM	NA	[13]
$\{[Cd_3(L)_2(bbi)_2(H_2O)_2]\cdot 2H_2O\}$	NFZ	1.83 ppm	8.26×10^3 M^{-1}	[14]
$\{[Tb\text{-}(HL)(H_2O)_2]\cdot_x(solv)\}_n$	NFT	NFT: 0.41 μM	NFT: 1.9×10^4 M^{-1}	[15]
$[Cd_7(SO_4)_6(tppe)_2](2DMF\cdot 2H_2O)$	NFZ	NA	1.7×10^3 M^{-1}	[16]
$[Eu(H_2O)(BTCTB)]\cdot 2H_2O$	NFT and NFZ	NFT: 0.60 μM NFZ: 0.67 μM	NFT: 2.1×10^4 M^{-1} NFZ: 1.27×10^4 M^{-1}	[17]
$[[Y_{0.9}Tb_{0.1}Sr(PDA)_3(H_2O)_4]\cdot Him\cdot 3H_2O$	NFT, NFZ and FRZ	NFZ: 0.49 μM NFT: 0.83 μM NFZ: 0.71 μM	NFZ: 5.35×10^4 M^{-1} NFT: 3.71×10^4 M^{-1} FRZ: 2.93×10^4 M^{-1}	Our work

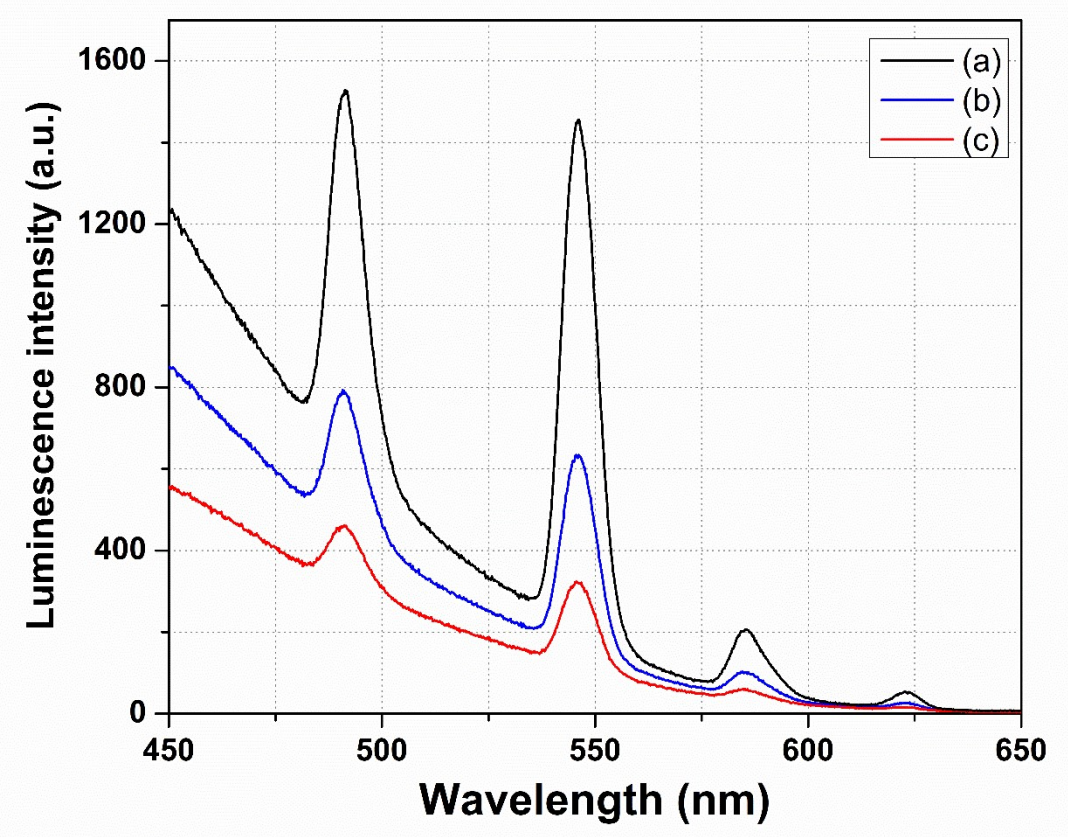

Fig. S24: Emission spectra of compound **1:Tb** in pond water upon spiked of (a) 0 μM (b) 30 μM (c) 50 μM NFZ solution (λ_{ex} = 280 nm).

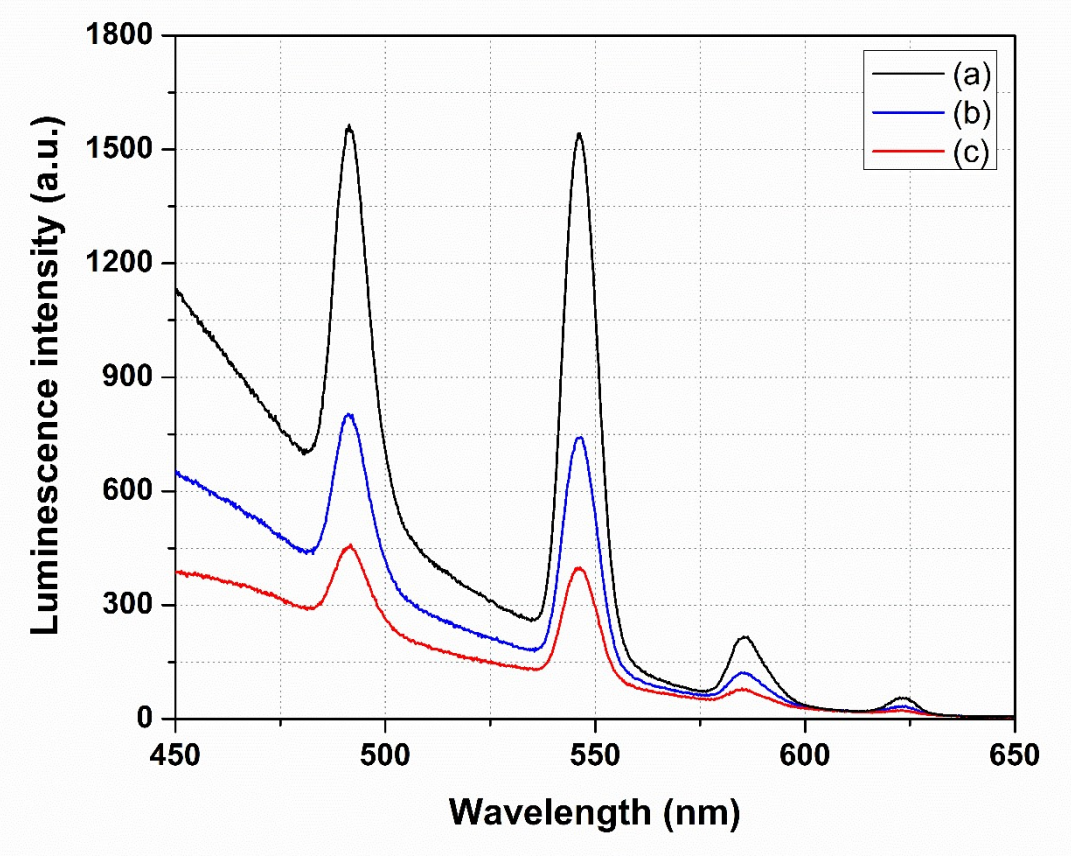

Fig. S25: Emission spectra of compound **1:Tb** in pond water upon spiked of (a) 0 µM (b) 30 µM (c) 50 µM NFT solution (λ_{ex} = 280 nm).

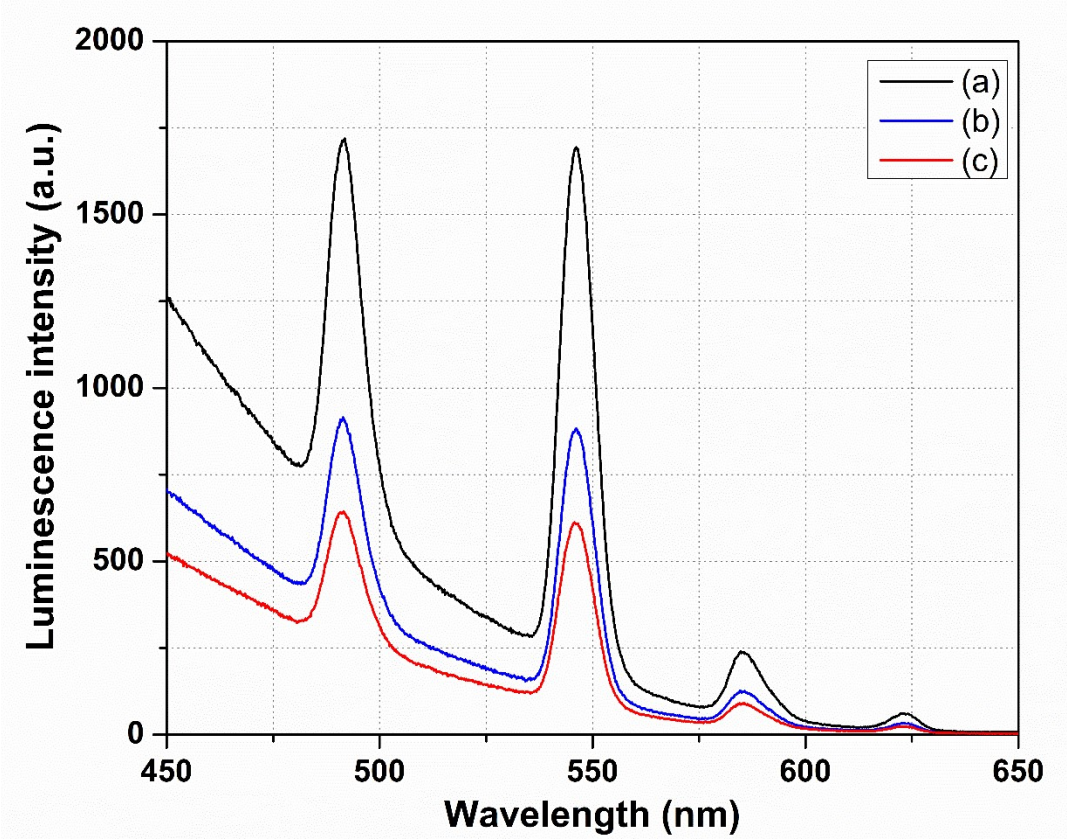

Fig. S26: Emission spectra of compound **1:Tb** in pond water upon spiked of (a) 0 µM (b) 30 µM (c) 50 µM FRZ solution (λ_{ex} = 280 nm).

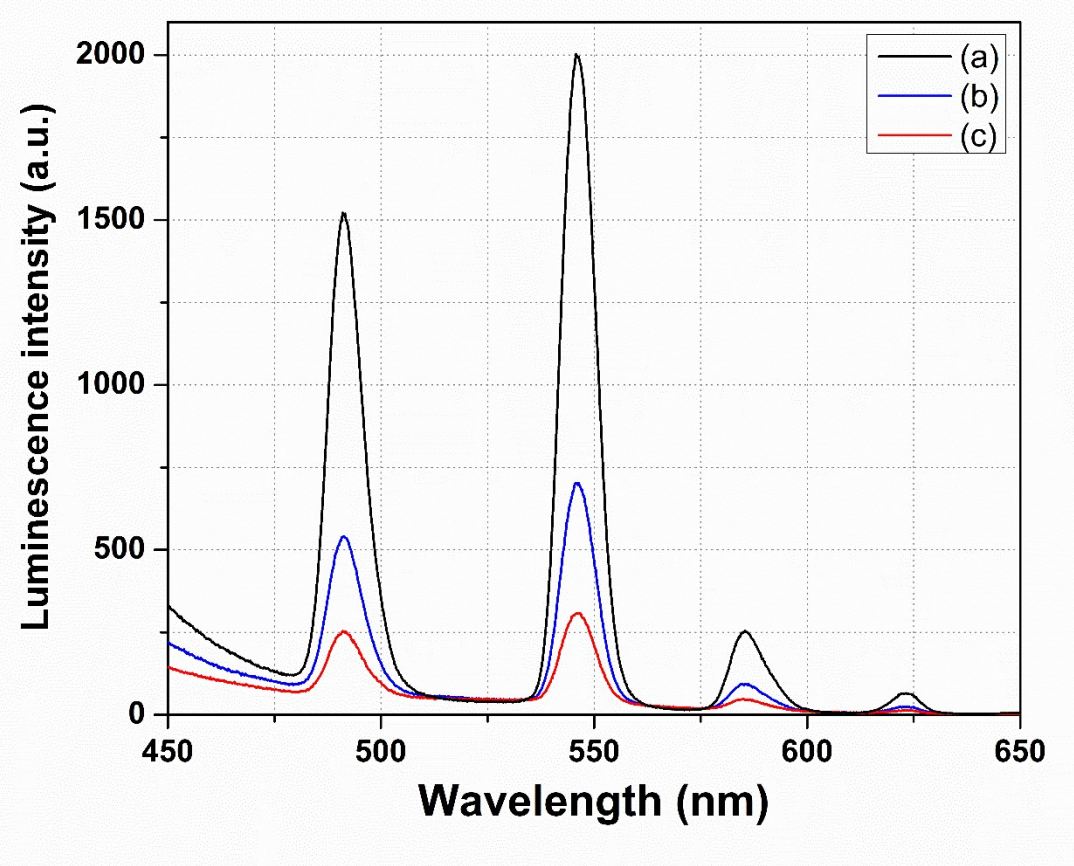

Fig. S27: Emission spectra of compound **1:Tb** in tap water upon spiked of (a) 0 μM (b) 30 μM (c) 50 μM NFZ solution (λ_{ex} = 280 nm).

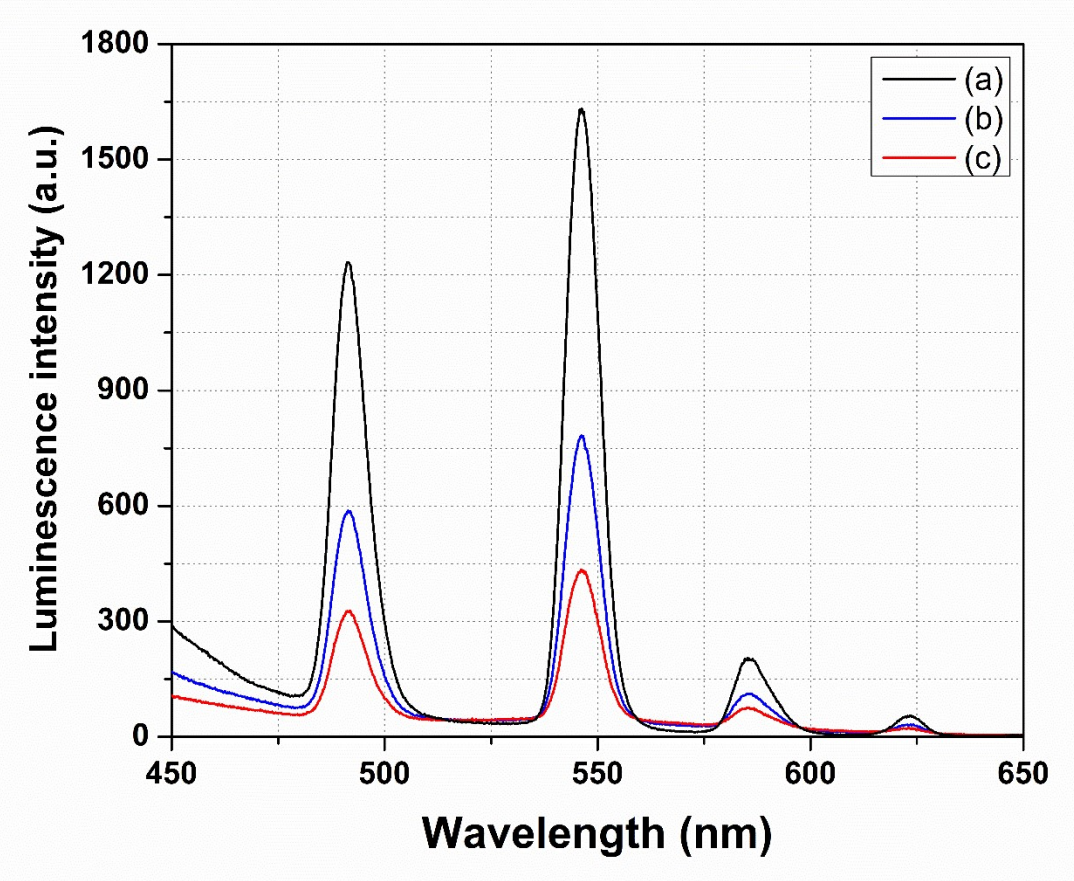

Fig. S28: Emission spectra of compound **1:Tb** in tap water upon spiked of (a) 0 μM (b) 30 μM (c) 50 μM NFT solution (λ_{ex} = 280 nm).

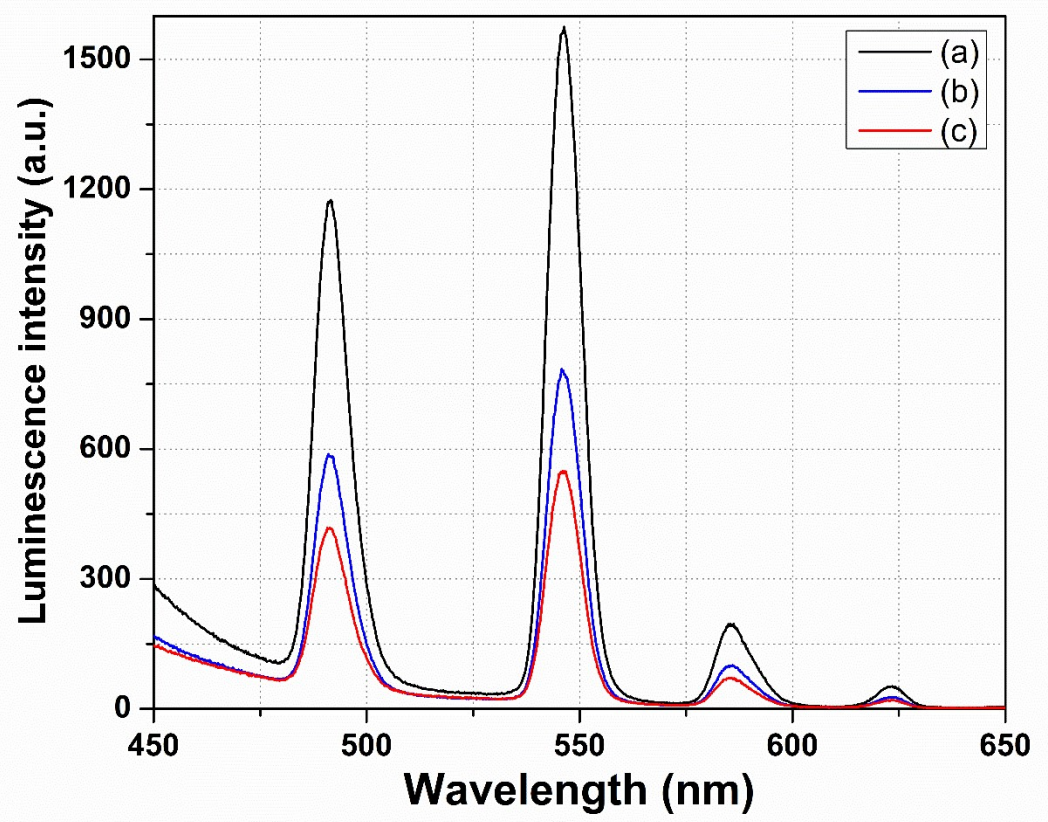

Fig. S29: Emission spectra of compound **1:Tb** in tap water upon spiked of (a) 0 μM (b) 30 μM (c) 50 μM FRZ solution (λ_{ex} = 280 nm).

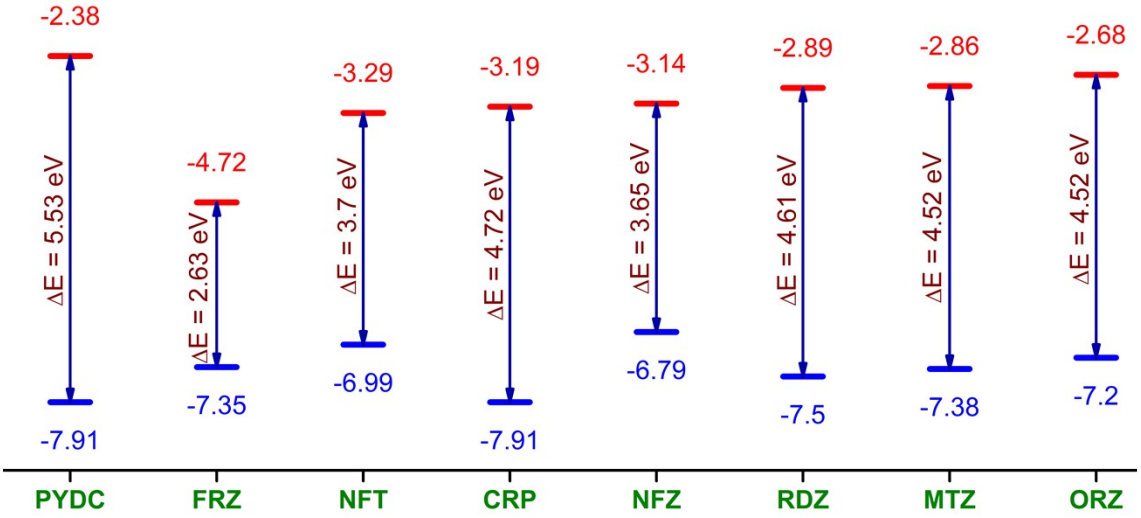

Fig. S30: The estimated HOMO LUMO energy values of the 2,6-pydc ligands and tested antibiotics.

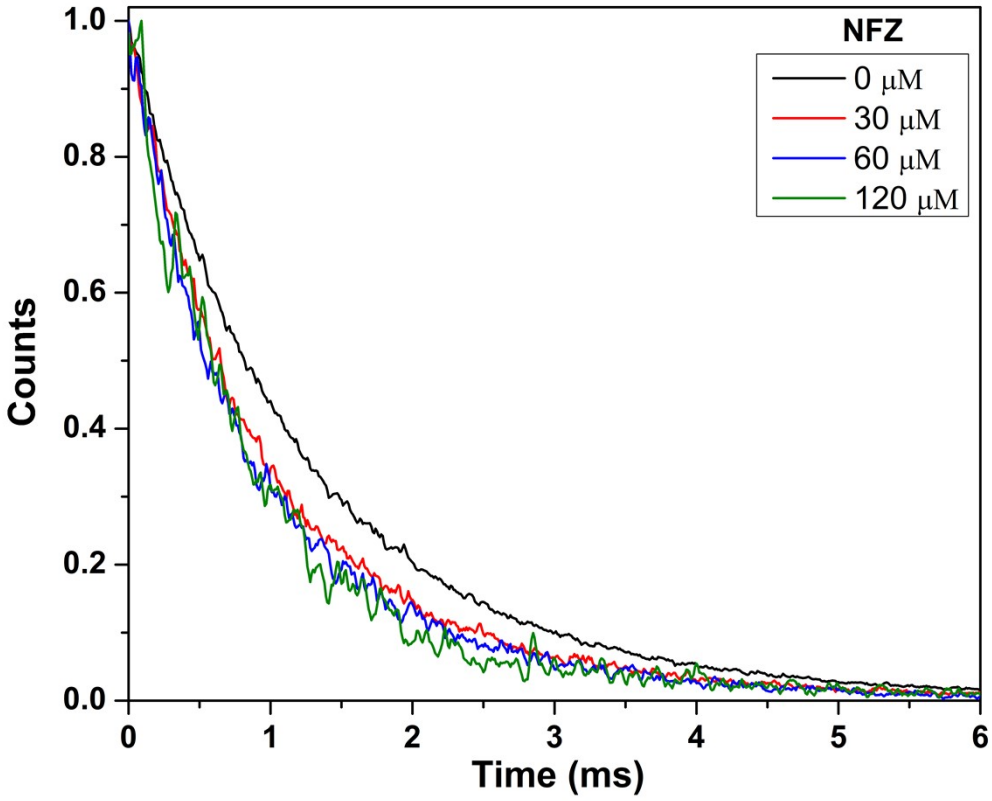

Fig. S31: Luminescence lifetime decay curve of compound **1:Tb** (at 545 nm) upon addition of NFZ.

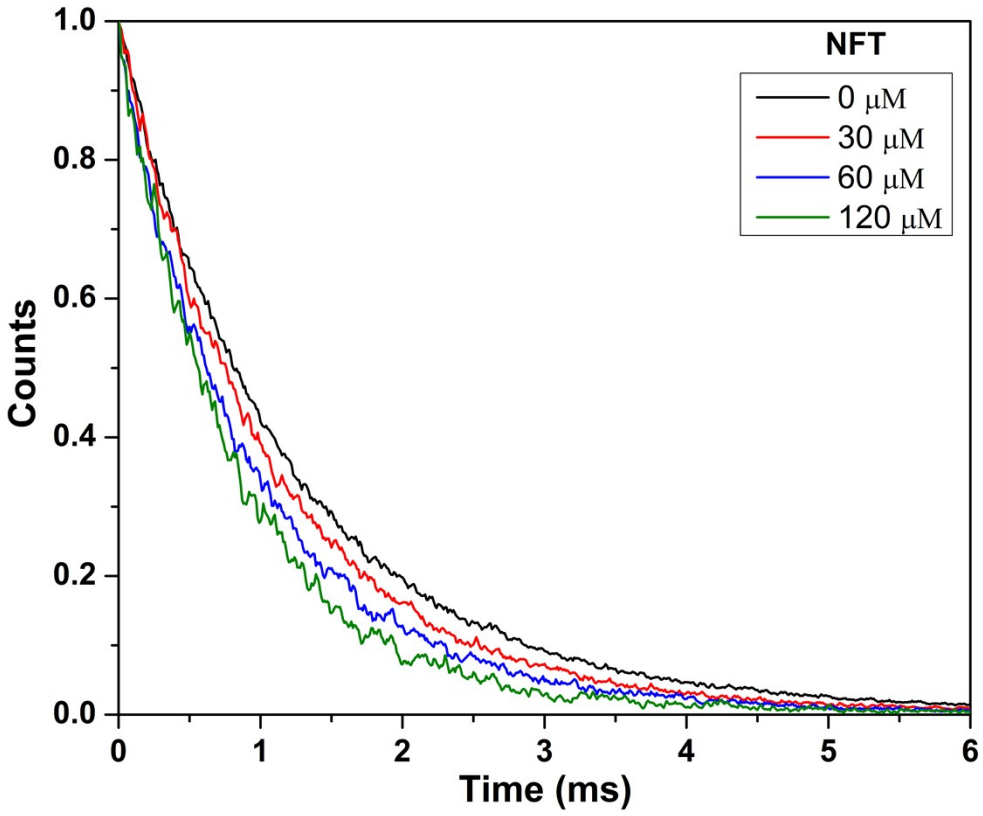

Fig. S32: Luminescence lifetime decay curve of compound **1:Tb** (at 545 nm) upon addition of NFT.

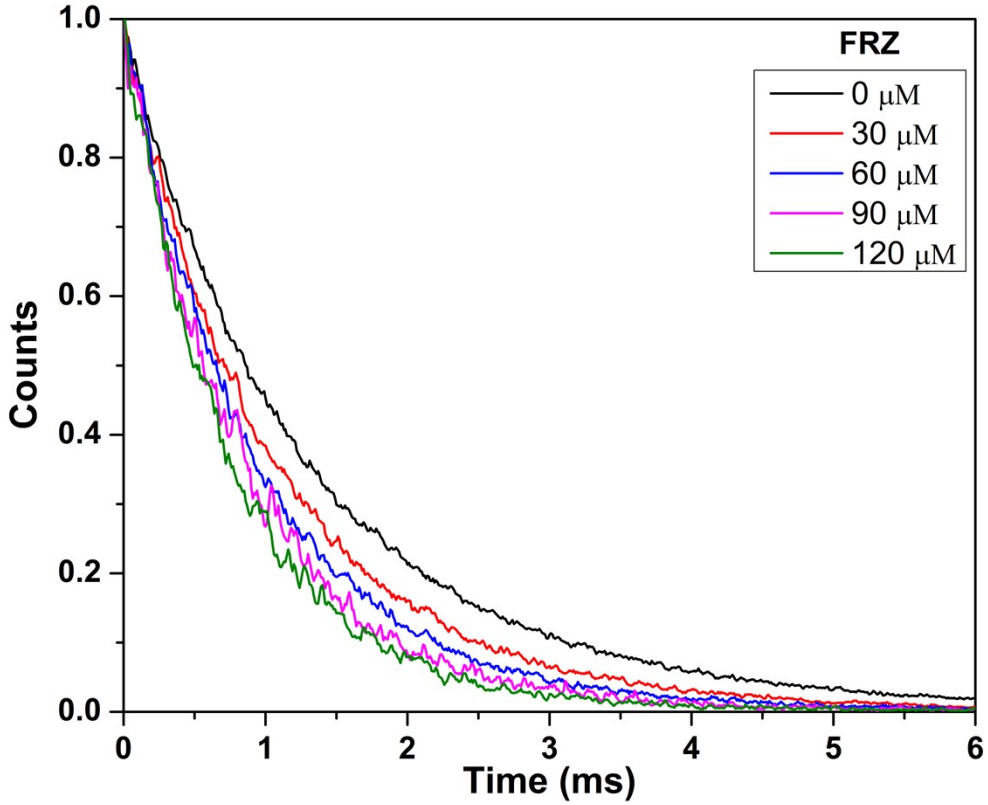

Fig. S33: Luminescence lifetime decay curve of compound **1:Tb** (at 545 nm) upon addition of FRZ.

References:

1. Apex3 v2017.3-0, Saint V8.38A, SAINT V8.38A, 2018).
2. L. Krause, R. Herbst-Irmer, G. M. Sheldrick and D. Stalke, Comparison of silver and molybdenum microfocus X-ray sources for single-crystal structure determination, *J. Appl. Crystallogr.*, 2015, **48**, 3-10.
3. A. Altomare, G. Cascarano, C. Giacovazzo and A. Guagliardi, Completion and refinement of crystal structures with SIR92, *J. Appl. Crystallogr.*, 1993, **26**, 343-350.
4. G. M. Sheldrick, Crystal structure refinement with SHELXL, *J Acta CrystallographicaSection C: Structural Chemistry*, 2015, **71**, 3-8.
5. L. J. Farrugia, WinGX suite for small-molecule single-crystal crystallography, *J. Appl. Crystallogr.*, 1999, **32**, 837-838.
6. A. Spek, Single-crystal structure validation with the program PLATON, *J. Appl. Crystallogr.*, 2003, **36**, 7-13.
7. F. Zhang, H. Yao, Y. Zhao, X. Li, G. Zhang and Y. Yang, Mixed matrix membranes incorporated with Ln-MOF for selective and sensitive detection of nitrofuran antibiotics based on inner filter effect, *Talanta*, 2017, **174**, 660-666.
8. M. Yu, Y. Xie, X. Wang, Y. Li and G. Li, Highly Water-Stable Dye@Ln-MOFs for Sensitive and Selective Detection toward Antibiotics in Water, *ACS Appl. Mater. Interfaces*, 2019, **11**, 21201-21210.
9. H. He, Q.-Q. Zhu, C.-P. Li and M. Du, Design of a Highly-Stable Pillar-Layer Zinc(II) Porous Framework for Rapid, Reversible, and Multi-Responsive Luminescent Sensor in Water, *Cryst. Growth Des.*, 2019, **19**, 694-703.
10. Z.-W. Zhai, S.-H. Yang, M. Cao, L.-K. Li, C.-X. Du and S.-Q. Zang, Rational Design of Three Two-Fold Interpenetrated Metal–Organic Frameworks: Luminescent Zn/Cd-Metal–Organic Frameworks for Detection of 2,4,6-Trinitrophenol and Nitrofurazone in the Aqueous Phase, *Cryst. Growth Des.*, 2018, **18**, 7173-7182.
11. Q.-Q. Zhu, Q.-S. Zhou, H.-W. Zhang, W.-W. Zhang, D.-Q. Lu, M.-T. Guo, Y. Yuan, F. Sun and H. He, Design and Construction of a Metal–Organic Framework as an Efficient Luminescent Sensor for Detecting Antibiotics, *Inorg. Chem.*, 2020, **59**, 1323-1331.
12. Y. Zhang, J. Yang, D. Zhao, Z. Liu, D. Li, L. Fan and T. Hu, Two cadmium(ii) coordination polymers as luminescent sensors for the detection of nitrofuran/nitroimidazole antibiotics, *CrystEngComm*, 2019, **21**, 6130-6135.
13. Y. Yang, G. Ren, W. Yang, X. Qin, D. Gu, Z. Liang, D.-Y. Guo and P. Qinhe, A new MOF-based fluorescent sensor for the detection of nitrofuran antibiotics, *Polyhedron*, 2021, **194**, 114923.
14. S. Zhou, L. Lu, D. Liu, J. Wang, H. Sakiyama, M. Muddassir, A. Nezamzadeh-Ejhieh and J. Liu, Series of highly stable Cd(ii)-based MOFs as sensitive and selective sensors for detection of nitrofuran antibiotic, *CrystEngComm*, 2021, **23**, 8043-8052.
15. M. Lei, F. Ge, X. Gao, Z. Shi and H. Zheng, A Water-Stable Tb-MOF As a Rapid, Accurate, and Highly Sensitive Ratiometric Luminescent Sensor for the Discriminative Sensing of Antibiotics and D2O in H2O, *Inorg. Chem.*, 2021, **60**, 10513-10521.
16. Y. Zhao, Y.-J. Wang, N. Wang, P. Zheng, H.-R. Fu, M.-L. Han, L.-F. Ma and L.-Y. Wang, Tetraphenylethylene-Decorated Metal–Organic Frameworks as Energy-Transfer Platform for the Detection of Nitro-Antibiotics and White-Light Emission, *Inorg. Chem.*, 2019, **58**, 12700-12706.
17. H.-W. Yang, P. Xu, B. Ding, Z.-Y. Liu, X.-J. Zhao and E.-C. Yang, A Highly Stable Luminescent Eu-MOF Exhibiting Efficient Response to Nitrofuran Antibiotics through the Inner Filter Effect and Photoinduced Electron Transfer, *Eur. J. Inorg. Chem.*, 2019, **2019**, 5077-5084.